



## OPEN ACCESS

## EDITED BY

Guangzhao Wang,  
Yangtze Normal University, China

## REVIEWED BY

Kai Ren,  
Nanjing Forestry University, China  
Jian Yang,  
Kunming University of Science and  
Technology, China

## \*CORRESPONDENCE

Cheng Zhan,  
✉ czhan@njjust.edu.cn  
Xiangyu Zhu,  
✉ zhuxiangyu@njjust.edu.cn

RECEIVED 17 January 2025

ACCEPTED 24 February 2025

PUBLISHED 19 March 2025

## CITATION

Sun X, Zhu X, Kan E and Zhan C (2025) A  
first-principles density functional theory study  
on the piezocatalytic activity of tetragonal  
perovskite  $\text{PbTiO}_3$ .  
*Front. Phys.* 13:1562239.  
doi: 10.3389/fphy.2025.1562239

## COPYRIGHT

© 2025 Sun, Zhu, Kan and Zhan. This is an  
open-access article distributed under the  
terms of the [Creative Commons Attribution  
License \(CC BY\)](https://creativecommons.org/licenses/by/4.0/). The use, distribution or  
reproduction in other forums is permitted,  
provided the original author(s) and the  
copyright owner(s) are credited and that the  
original publication in this journal is cited, in  
accordance with accepted academic practice.  
No use, distribution or reproduction is  
permitted which does not comply with  
these terms.

# A first-principles density functional theory study on the piezocatalytic activity of tetragonal perovskite $\text{PbTiO}_3$

Xinyi Sun<sup>1,2,3</sup>, Xiangyu Zhu<sup>1,2,3\*</sup>, Erjun Kan<sup>1,2,3</sup> and  
Cheng Zhan<sup>1,2,3\*</sup>

<sup>1</sup>MIT Key Laboratory of Semiconductor Microstructure and Quantum Sensing, Nanjing University of Science and Technology, Nanjing, China, <sup>2</sup>School of Physics, Nanjing University of Science and Technology, Nanjing, China, <sup>3</sup>Engineering Research Center of Semiconductor Device Optoelectronic Hybrid Integration in Jiangsu Province, Nanjing University of Science and Technology, Nanjing, China

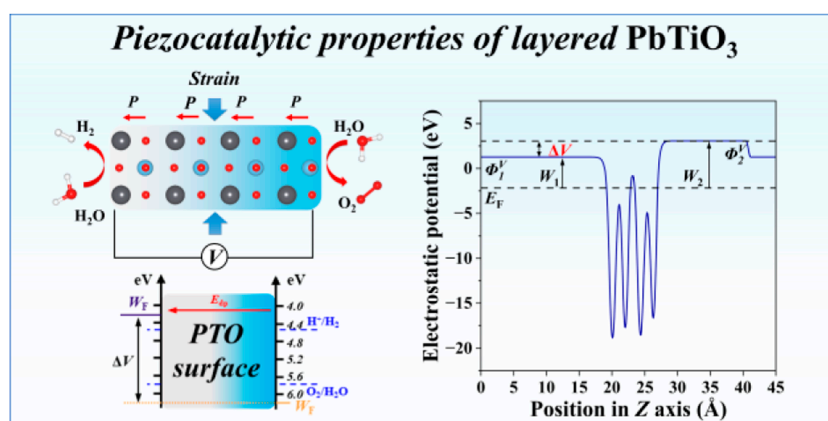
Piezoelectric materials have been found to possess high catalytic activity under external mechanical excitations, such as ultrasonic waves or collisions. Energy band theory (EBT) based on electronic excitation in semiconductors has been widely used to investigate piezocatalytic activity from a macroscopic perspective, while the microscopic correlation between the piezoelectric feature and surface chemical reactivity was not fully understood at the current stage. In this work, to overcome the limitation of conventional finite element modeling of piezoelectric materials, we employ the first-principles density functional theory (DFT) to study the electronic properties, macroscopic electrostatic potential, surface polarization, and chemical adsorption energy of tetragonal  $\text{PbTiO}_3$  under external mechanical strains. The correlations between the band structure, piezopotential, space charge distribution, and surface adsorption energy of the  $^*\text{OH}/\text{H}$  groups are discussed in our work. Our simulation shows that the bulk PTO and layered PTO exhibit opposite trends in the band gap change under external strain. In addition, a nonmonotonic correlation between the change of dipole moment piezopotential versus the applied strain was found in few-layer PTO, which could directly quantify the driving force of piezocatalysis. Finally, the enhanced surface adsorption of  $^*\text{OH}$  and  $^*\text{H}$  on PTO was observed under both tensile and compressive strain, which reveals how piezoelectric features affect the surface chemical process in thermodynamics. Our work provides a significant mechanistic insight into the piezocatalytic behavior of general polar perovskite, which could facilitate the development of piezoelectric materials in energy conversion and environmental applications.

## KEYWORDS

piezocatalysis, density functional theory, perovskite, water splitting, surface chemistry

## Introduction

Energy harvesting and conversion technologies have received tremendous attention in recent decades due to the increasing energy consumption as well as serious environmental



GRAPHICAL ABSTRACT

problems [1–5]. Direct utilization of energy from the natural environment is an effective way to deal with energy and environmental problems. In addition to the most well-known photovoltaic technology that can directly convert solar energy from nature into electricity, energy conversion via the piezoelectric effect is another way to exploit natural energy that can convert mechanical energy into electricity or chemical energy [6–8]. According to the fundamental concept of electrostatics and electrochemistry, a large electrical potential drop on a material surface can govern the electrochemical reaction and electron transfer. The concept of “piezocatalysis” was proposed based on the electrocatalytic process induced by a large potential drop on the piezo-electrified surface [9]. This phenomenon has been validated in many experimental studies. For instance, Hong et al. discovered piezocatalytic water splitting on the ZnO fiber and BaTiO<sub>3</sub> dendrite, which could generate oxygen and hydrogen gas from pure water in a stoichiometric ratio under the excitation of ultrasonic vibration [10]. Starr et al. made a similar observation in Pb(Mg<sub>1/3</sub>Nb<sub>2/3</sub>)O<sub>3</sub>-32PbTiO<sub>3</sub> (PMN-PT) material and reported the direct hydrogen generation induced by piezoelectric effects [11]. In addition to the water-splitting reaction, piezocatalysis has also been employed in pollutant degradation, medical cleaning, and organic synthesis [12–18].

To understand the mechanism of piezocatalysis, the energy band theory (EBT) was developed to interpret the driving force of the piezocatalytic process [19]. Due to the spontaneous polarization in piezoelectric materials and the effects of mechanical strain, the band edge usually exhibits a linear shift along the direction of polarization under the external strain [11, 20]. This effect causes the possible redox reaction that occurs when the modified band edge reaches the redox potential of chemical species on the surface. Under the frame of EBT, the driving force of piezocatalysis was attributed to electronic excitation by thermal effect during the vibrational excitation, which is highly similar to photocatalysis. This indicates that the piezopotential is determined by the band structure of the material under mechanical strain [21, 22]. Different from EBT, the screening charge effect (SCE) model was proposed based on the electrostatics of the piezo-electrified medium [19]. According to the SCE model, piezocatalysis is dominated by the presence of a screening charge on the electrified surface. With

the help of finite-element simulation, numerical solutions of the global electrostatic potential can be obtained at any mechanical strain, which clearly visualizes the polarity of the piezoelectric material [14, 23, 24]. The piezopotential is defined as the electrostatic potential difference between two sides and determines the size of the driving force of piezocatalysis [11, 22, 25]. Although EBT and SCE models have been extensively used to provide a mechanistic understanding of piezocatalysis from different physical scales and perspectives, the microscopic reaction process and mechanism on the surface of piezoelectric materials are not well understood. In addition, the intrinsic connection between EBT and SCE models is still blurry at the current stage, which limits further mechanistic investigation of piezocatalysis. To fully understand the mechanism of piezocatalysis, in this work, we take the typical piezoelectric perovskite PbTiO<sub>3</sub> (PTO) as an example and carry out the first-principles density functional theory (DFT) calculation to investigate the electronic structure, polarization, space charge distribution, and surface reactivity under mechanical strain. Our work could provide fundamental insights into the physical picture of piezocatalysis and further benefit the development of piezoelectric materials in renewable energy applications.

## Simulation method

Density functional theory calculations were carried out by using the Vienna *ab initio* Simulation Package (VASP) software [26, 27]. The ion–electron interaction was treated by the projector augmented-wave (PAW) pseudopotential [28]. The generalized gradient approximation with the Perdew–Burke–Erzerhof (GGA-PBE) formalism was used to describe the exchange–correlation effect [29, 30]. The plane-wave basis set with a cutoff energy of 550 eV was adopted to expand the wave function under periodic boundary conditions. The van der Waals (vdW) interaction was captured through Grimme’s DFT-D3 correction method [31]. The convergence criteria of geometric optimization and electronic iteration were set as 0.02 eV/Å and 10<sup>−5</sup> eV, respectively. The *k*-point sampling of the Brillouin zone was carried out using the Monkhorst–Pack scheme with the *k*-mesh resolution of 0.04 (in the

unit of  $2\pi/\text{\AA}$ ) [32]. To reasonably deal with the strong correlation effect of  $3d$  electrons, the GGA +  $U$  method was employed for Ti with the  $U$  value of 3.0 eV from early literature [33]. In addition, the hybrid functional calculation was also performed using the HSE06 formalism to obtain an accurate band structure and band gap [34, 35]. The surface slab model of the 2/3/4 layers  $\text{PbTiO}_3$  in the [001] direction was created in contact with a vacuum slab with a thickness of 40  $\text{\AA}$  to avoid the layer-layer interaction and reliably capture the dipole moment along the  $z$  direction. To investigate the effect of mechanical strain on the polarization and electronic properties in PTO, a biaxial strain was introduced on the equilibrated lattice, which has been validated as an effective strategy for understanding piezoelectric materials [22, 36, 37]. The mechanical strain ( $\delta$ ) was defined as  $\delta = (a - a_0)/a_0$ , where  $a_0$  and  $a$  refer to the equilibrated and compressed/stretched lattice constant, respectively. In addition, dipole correction was employed to treat the highly polarized surface in the electrostatic potential calculation because our test calculation has shown that the electrostatic potential is not able to converge in the center of the vacuum slab if dipole correction is not included, as shown in Supplementary Figure S1; [38].

The electronic polarization of PTO was calculated using the Berry phase method developed by King-Smith and Vanderbilt, which directly provides the electronic dipole moment in each direction [39]. The ionic part of polarization is directly defined by the ion valance and location, giving the expression of total polarization along the  $z$  direction as Equation 1:

$$P = P_{\text{ion}} + P_{\text{elec}} = \sum_i (r - r_0) Z_i(r) + P_{\text{elec}}, \quad (1)$$

where the first and second terms refer to the contribution of ionic and electronic dipole moment in the  $z$  direction. The  $r_0$ ,  $Z_i$  refers to the reference location and valence charge of ion along the  $z$  direction, respectively.  $P_{\text{elec}}$  is given by the Berry phase calculation.

## Results and discussion

### Effects of Hubbard $U$ and exchange-correlation functional on the geometry, polarization, electronic, and mechanical properties of bulk PTO

Because the accuracy of lattice parameters significantly affects the calculated polarization of ionic contribution, different functionals were tested as a comparison, including PBE [30], PBEsol [40], and HSE06 [34], with and without Hubbard correction, as listed in Table 1. The calculated structure parameters, polarization, and mechanical properties were compared with previous experimental results. As listed in Table 1, our simulation indicates that PBE +  $U$  shows good consistency with experimental data in structural parameters and polarization charge density  $P_s$ , whereas PBE, PBEsol, and HSE06 overestimate  $P_s$ . Conversely, PBEsol +  $U$  underestimates the  $P_s$  value, which suggests that the introduction of Hubbard  $U$  could lower the calculated  $P_s$ . However, the introduction of Hubbard  $U$  makes the mechanical property calculation worse than the experimental results. Additionally, PBEsol predicts the band gap as 1.61 eV, which significantly underestimates the band gap compared with the HSE06 ( $E_g = 3.05$  eV) and experimental data ( $E_g$

= 3.10 eV). Early DFT study has indicated that applying the Hubbard  $U$  correction could push the Ti ( $3d$ ) states to be more localized on Ti ions, which significantly affects the length of the Ti–O bond along [001] direction and the ionic polarization [41]. Our results similarly find that the Hubbard  $U$  suppresses Ti ( $3d$ )–O ( $2p$ ) hybridization (Supplementary Figure S2) and leads to a smaller  $c$  parameter than PBE and PBEsol. Because the piezocatalytic activity in PTO is dominated by mechanical excitation in the planar direction ( $x$  and  $y$  direction) and polarization response in the vertical direction ( $z$  direction), it is important to accurately capture the effects of in-plane strain ( $x/y$  direction, which is related to  $C_{11}$ ,  $C_{12}$ , and  $C_{13}$ ) on the electronic structure and polarization. Thus, to obtain a reliable result on the polarization property under in-plane strain, we will employ the PBE +  $U$  calculation for geometry optimization and polarization calculation, which has exhibited reasonable accuracy compared with early experimental results [42–44]. The electronic structure and band gap will be calculated via HSE06 based on a single-point calculation after structure optimization by PBE +  $U$ .

### Effects of mechanical strain on the band structure

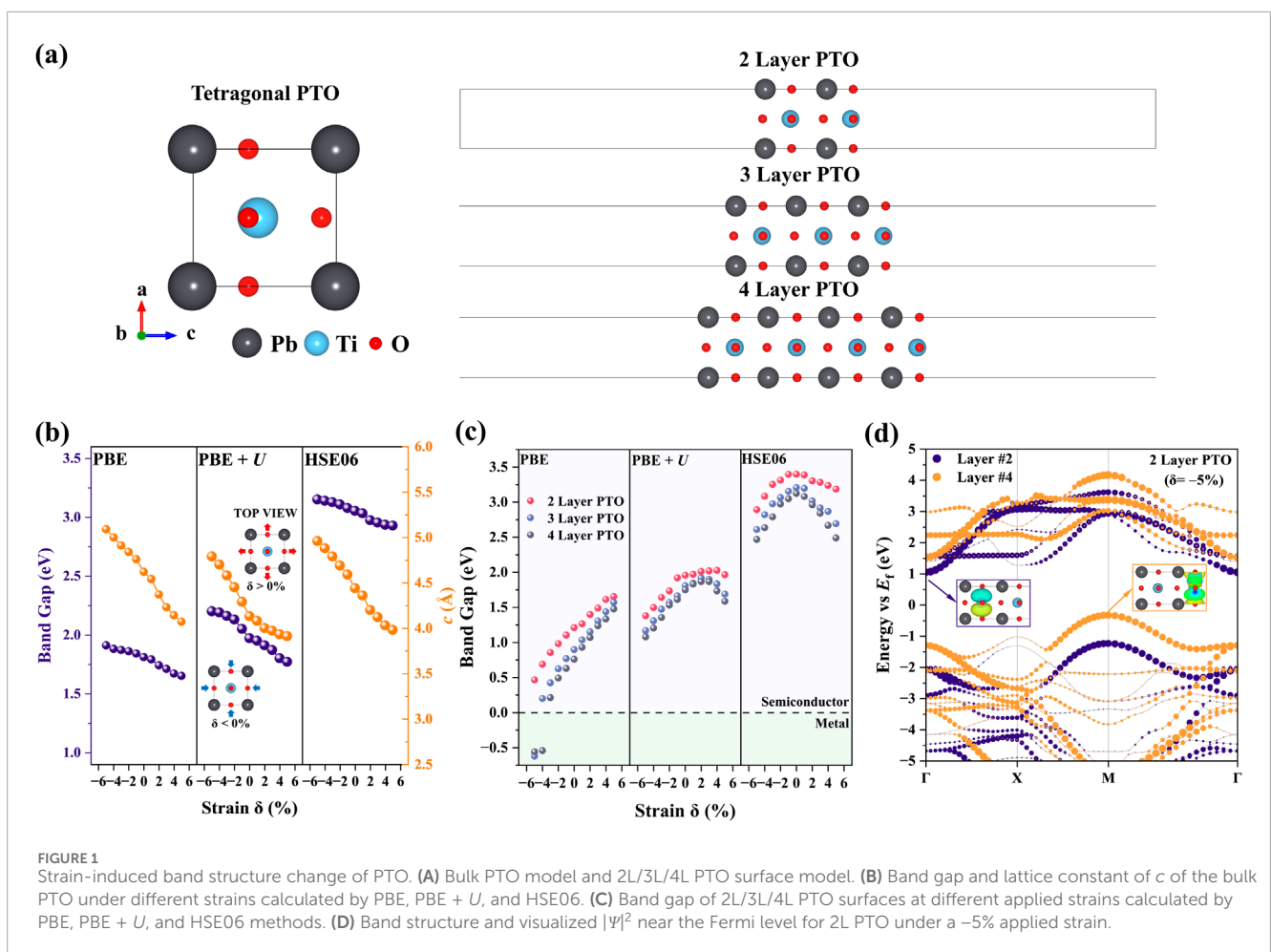
To understand the change of electronic structure under piezoelectric polarization, we first studied the band structure of bulk PTO under biaxial strain on the lattice, as shown in Supplementary Figures S3, S4. We compared the band structure calculation results from PBE, PBE +  $U$ , and HSE06 functionals in Supplementary Figure S3. It shows that all the methods predicted the bulk PTO as an indirect semiconductor with the valence band maximum (VBM) located at X and the conduction band minimum (CBM) located at the  $\Gamma$  and Z points. The flat region of the conduction band in the K-path ( $\Gamma$  to Z) is also consistent with an early study by Bendaoudi et al. [37]. The HSE06 predicts the  $E_g$  of bulk PTO as 3.05 eV, which is very close to the experimentally measured  $E_g = 3.10$  eV, while PBE and PBE +  $U$  predict the  $E_g = 1.81$  eV and  $E_g = 1.97$  eV, respectively. (Figure 1B). The band structure of PTO from PBE +  $U$  and HSE06 is like the  $\text{BaTiO}_3$  in our previous work [22].

As shown in Figure 1B and Supplementary Figure S4, with the introduction of biaxial strain ( $\delta = -5\%$  to  $+5\%$ ), we observed a monotonic variation of  $E_g$  with the strain with the PBE, PBE +  $U$ , and HSE06. Under a compressive strain of  $\delta = -5\%$ ,  $E_g$  increases to 2.20 eV, while  $E_g$  decreases to 1.77 eV when a tensile strain of  $\delta = +5\%$  is introduced along the lattice vector  $a$  in the  $xy$  plane. The projected density of states (PDOS) (Supplementary Figure S5) indicates that the CBM is primarily contributed by Ti, while the VBM is mainly contributed by O. Compressive strain causes a displacement of the Ti ion from its centrosymmetric position, leading to polarity change. This structural distortion enhances the hybridization between the Ti- $3d$  and O- $2p$  orbitals, thus increasing the VBM-CBM energy difference and leading to a wider band gap. Berger et al. also reported the effect of polarity change on the band gap [47]. The location of VBM and CBM remain unchanged under the compressive and tensile strain on bulk PTO.

To explore the piezoelectric effects on the band structure of PTO under realistic experimental conditions, we established the few-layer PTO model shown in Figure 1A. The PTO surface model was built

**TABLE 1** Calculated lattice parameters (in Å), spontaneous polarization ( $P_s$  in C/m<sup>2</sup>), band gap ( $E_g$  in eV), and elastic constants (in GPa). Experimental results were taken from early literature [42–46].

	$a$	$c$	$P_s$	$E_g$	$C_{11}$	$C_{12}$	$C_{13}$	$C_{33}$	$C_{44}$	$C_{66}$
PBE	3.84	4.62	1.19	1.87	203.11	91.00	67.31	60.88	58.69	94.98
PBE + $U$	3.95	4.13	0.76	1.91	239.90	92.93	60.82	22.84	73.60	96.16
PBEsol	3.87	4.14	0.88	1.61	264.12	109.81	92.14	96.25	54.85	98.33
PBEsol + $U$	3.92	4.00	0.59	1.78	302.75	120.61	107.56	157.63	60.48	95.61
HSE06	3.83	4.44	1.16	3.05	234.71	94.52	62.23	35.41	56.71	108.04
Exp	3.90 [42]	4.16 [42]	0.76 [43]	3.10 [45, 46]	235 [44]	105 [44]	101 [44]	98 [44]	65 [44]	104 [44]



along the (001) direction of the bulk PTO, and we created three PTO surface models: 2L-, 3L-, and 4L-PTO, which are shown in Figure 1A. The effect of biaxial strain on the  $E_g$  of 2L/3L/4L PTO is systematically studied in Figure 1C. Compared with the results of bulk PTO (Figure 1B), the few-layer PTO shows an opposite trend in the  $E_g$ - $\delta$  relation, as shown in Figure 1C. The  $E_g$  of few-layer PTO shows a nonmonotonic trend with the mechanical strain that varies from compressive (-5%) to tensile (+5%). In Figure 1C,

the HSE06 results show that compressive or tensile strain both decrease the  $E_g$ , leading to a “bell” shape in the  $E_g$ - $\delta$  relation. Interestingly, PBE +  $U$  predicts a slightly decreased  $E_g$  in the tensile strain region, while PBE results show a monotonically increasing  $E_g$  with  $\delta$ . The opposite trend given by PBE in the tensile strain region suggests that the strong correlation effect of 3d electron in Ti plays a crucial role in determining the band gap of the tensile PTO surface. We visualized the wavefunction of 2L PTO at VBM

(M point) and CBM ( $\Gamma$ ) in Figure 1D, which shows that the VBM and CBM were both contributed by the  $\text{TiO}_2$  layer.

According to the projected density of states (PDOS) analysis in Supplementary Figure S6, it can be seen that the CBM of the PTO surface is mainly dominated by the O, while the CBM is mainly contributed by Ti. To validate the contribution of each layer in the band structure, we further decomposed the band in the real space in Supplementary Figure S7 (layer index definition) and Supplementary Figure S8 (layer-resolved band structure). It can be clearly found that the CBM and VBM are contributed by layer 2 (inner  $\text{TiO}_2$  layer) and layer 4 (surface  $\text{TiO}_2$  layer), respectively, while layer 1 (surface PbO layer) and layer 3 (inner PbO layer) make little contribution. This situation is not affected by the introduction of mechanical strain, as shown in Supplementary Figure S9. Compared with our previous study on BTO [22], our simulation of PTO exhibits a decreasing  $E_g$  under the tensile strain, which might weaken the driving force of piezocatalysis according to the EBT.

## Space charge redistribution and strain-induced polarization response

Because the polarization is determined by the charge distribution inside the material, to understand the polarization of PTO, we investigated the distribution of atomic charge in bulk and few-layer PTO. The Bader charge [48] was used to describe the atomic charge and further calculate the layer-resolved charge transfer. As shown in Figure 2A, in bulk PTO, according to the sum of Bader charge, the  $\text{TiO}_2$  layer gains  $0.2 e^-$  from the PbO layer, leading to the  $\text{TiO}_2$  node holding a  $-0.2 |e|$  charge and PbO node holding a  $+0.2 |e|$  charge. Under the compressive strain, the PbO layer sucks back  $0.04 e^-$  from the  $\text{TiO}_2$  layer, leading to the partial charge decreasing to  $-0.16 |e|$  on the  $\text{TiO}_2$  layer. However, under tensile strain, we observed the  $0.01 e^-$  electron transfer from the PbO to the  $\text{TiO}_2$  layer, leading to the  $-0.21 |e|$  partial charge on the  $\text{TiO}_2$  node.

We chose the bulk PTO as a reference and evaluated the partial charge distribution of few-layer PTO in Figure 2B. Comparing the few-layer PTO and bulk PTO under zero strain, a partial electron suck back to PbO layers was observed (cyan bar in Figure 2B) in 2L- and 4L-PTO. Electron accumulation was observed in layers 1/3 in 2L PTO and layers 1/3/5 in 4L PTO, while electron loss was observed in layer 4 in 2L-PTO, layer 6 in 3L-PTO, and layers 4/6/7 in 4L-PTO. This reverse electron transfer can be explained by the effect of depolarization. When extracting few-layer PTO from the bulk, electron transfer occurs due to the suddenly disappearing constraint from the macroscopic polarization of the whole system. This electron transfer usually tends to weaken the polarization, leading to the electron transfer from the negatively charged node ( $\text{TiO}_2$ ) to the positively charged node (PbO). With the introduction of strain, a relatively larger variation of space charge was observed in the compressive strain rather than tensile strain, as shown in Figure 2B. This can be explained by the change of Ti-O bond length under strain in Figure 2D: compressive strain pushes the O of the PbO layer and the Ti of the  $\text{TiO}_2$  layer to be closer, while tensile strain enlarges the Ti-O distance. The closer contact of Ti and O causes

more electron transfer, leading to a stronger degree of space charge redistribution.

The change of total dipole moment *versus* mechanical strain was also studied, as shown in Figure 2C. Interestingly, all the few-layer PTO models show enhanced polarization under compressive strain and weakened polarization under tensile strain. Although the space charge distribution shows that the electron transfer under compressive strain should decrease the polarization, an increase in dipole moment was still observed. This suggests that the contribution of the ionic dipole moment is more dominant than the electronic dipole moment in total dipole moment change. In addition, under the same degree of strain, a thicker layer exhibits larger dipole moment variation than a thin layer PTO. This finding indicates that the increase of overall polarization from the additional PTO layer cannot be perfectly counterbalanced by the depolarization field. The stronger polarization enhancement under strain in thicker layer PTO also suggests a stronger driving force of piezocatalysis, which will be discussed in the next section.

We also investigated the correlation between the band gap and dipole moment of 4L PTO, as shown in Supplementary Figure S10. It shows that there is a linear correlation between polarization and the variation of  $E_g$  under lattice strain. Specifically, Supplementary Figure S10 highlights that under compressive strain, a negative correlation is observed, while under tensile strain, a positive correlation emerges, with  $R^2$  values close to 1. This relationship aligns well with trends reported in previous literature [49, 50].

## Work function and piezopotential

Because the redox ability of a material under an external electric field or polarization is determined by the surface work function, we also investigated the work function of each side of PTO under various mechanical strains. Two vacuum references coexist due to the presence of dipole moment across the PTO along the  $z$  direction, which leads to different surface work functions on each side. As shown in Figure 3A, due to the negative charge accumulation on the  $\text{TiO}_2$  node, the upper side ( $\text{TiO}_2$  side on the right) possesses a larger work function than the lower side (PbO side on the left). We individually calculated the  $W_1$  and  $W_2$  at various strains, as shown in Figure 3B. It shows that both PBE +  $U$  and HSE06 predict a monotonically increasing  $W_1$  with strain  $\delta$ , while the  $W_2$  exhibits a fluctuating trend with the strain  $\delta$  changes from compressive to tensile, as shown in Figure 3B. In addition, HSE06 always predicts higher work function than PBE +  $U$ . Comparing the calculated work function with the energy level of redox potential of  $\text{O}_2$  and  $\text{H}_2$ , the HSE06 calculation shows that the work function of the  $\text{TiO}_2$  side is always beyond the oxidation potential of  $\text{H}_2\text{O}$  when  $\delta$  changes from  $-5\%$  to  $+5\%$ , while work function of the PbO side is below  $\text{H}^+/\text{H}_2$  redox potential only when the  $\delta$  decrease below  $-3\%$  in 2L-PTO. With the layer thickness increase to 3L and 4L, the work function  $W_1$  of the lower side tends to decrease, indicating a stronger driving force of hydrogen evolution reaction (HER) on the low potential side. In the 4L PTO, only a slight compressive strain of  $\delta = -1\%$  can push the  $W_1$  to below 4.5 eV (standard hydrogen electrode reference), while the  $W_2$  is still located beyond 5.73 eV ( $\text{H}_2\text{O}$  oxidation potential). This observation suggests that increasing

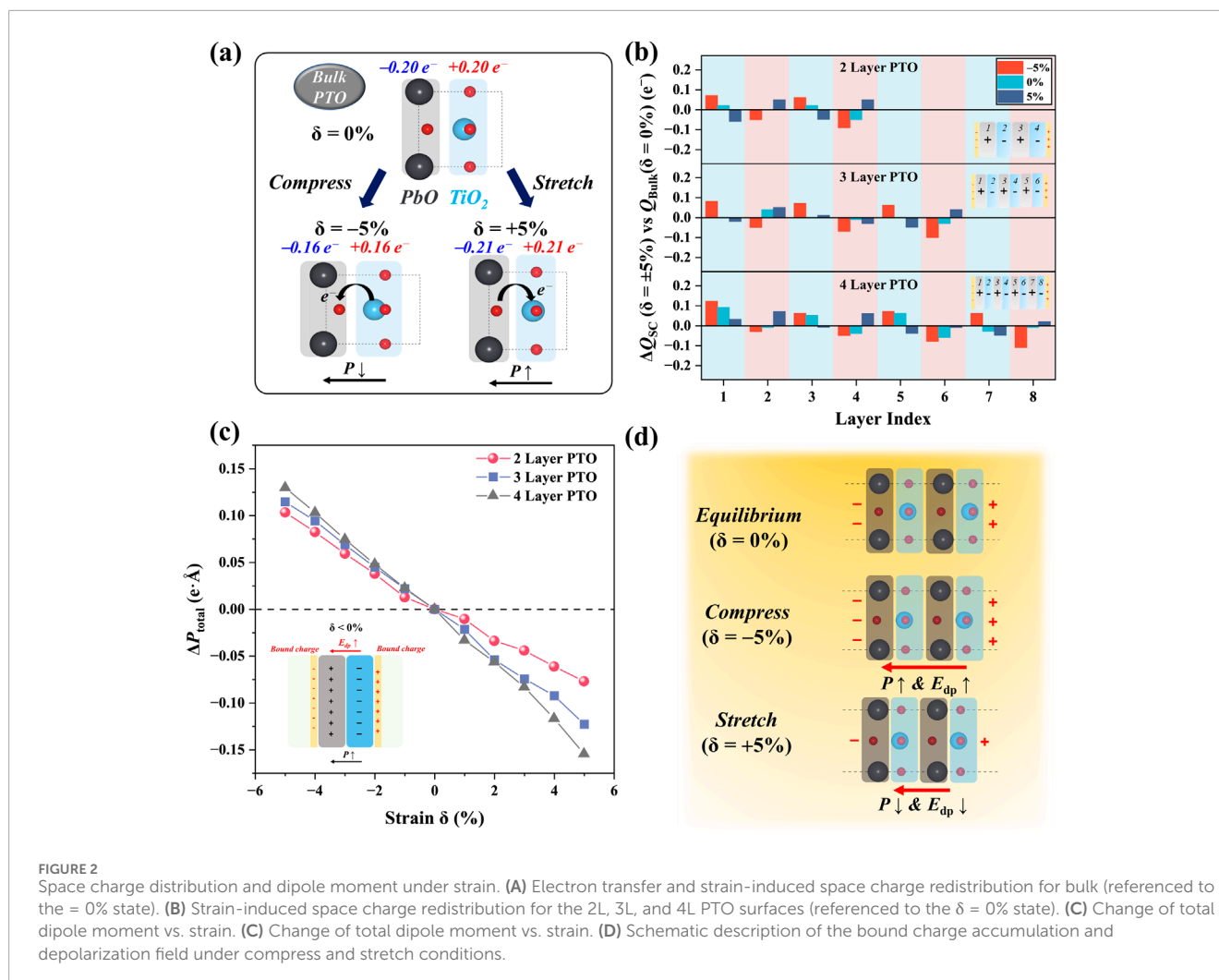


FIGURE 2

Space charge distribution and dipole moment under strain. (A) Electron transfer and strain-induced space charge redistribution for bulk (referenced to the  $\delta = 0\%$  state). (B) Strain-induced space charge redistribution for the 2L, 3L, and 4L PTO surfaces (referenced to the  $\delta = 0\%$  state). (C) Change of total dipole moment vs. strain. (D) Schematic description of the bound charge accumulation and depolarization field under compress and stretch conditions.

the PTO thickness could effectively benefit HER activity but have little influence on the driving force of OER.

We further calculated the potential difference between the PbO and  $TiO_2$  sides, which is defined as the piezopotential  $\Delta V$ . As shown in Figure 3C, we find that compressive strain increases  $\Delta V$  while tensile strain decreases  $\Delta V$ . This is consistent with the dipole moment change in Figure 2C, which indicates enhanced polarization by compressive strain and weakened polarization by tensile strain. In addition, the HSE06 method tends to predict a higher  $\Delta V$  than PBE +  $U$ , indicating the significance of a strong correlation effect in the simulation of the piezoelectric property. More importantly, with the layer number increase, we found a larger  $\Delta V$  variation under the same degree of mechanical strain, suggesting better activity in thicker PTO film. This observation is closely related to the depolarization field, which becomes more pronounced in thinner films and can partially suppress the net polarization and its associated potential. In thicker films, the depolarization field is effectively reduced, leading to a larger polarity and piezopotential. This phenomenon has been discussed from a theoretical approach [22, 51]. From the experimental perspective, promising piezocatalytic performance was usually observed in the thick PTO, which

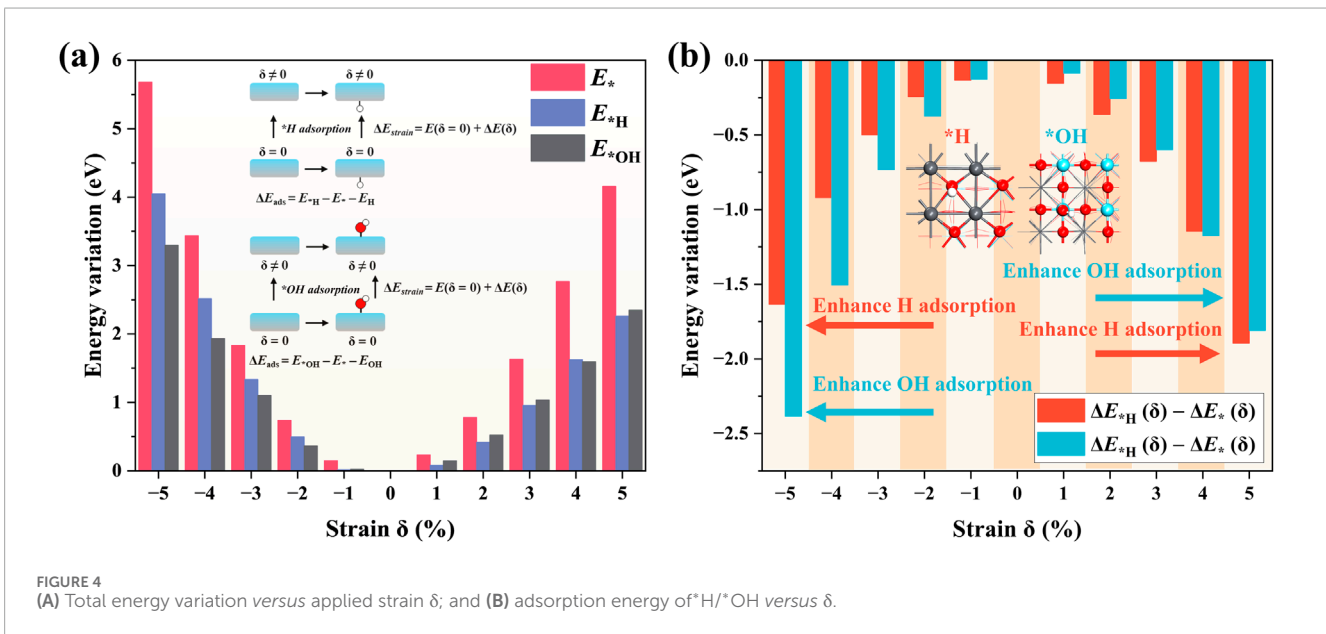
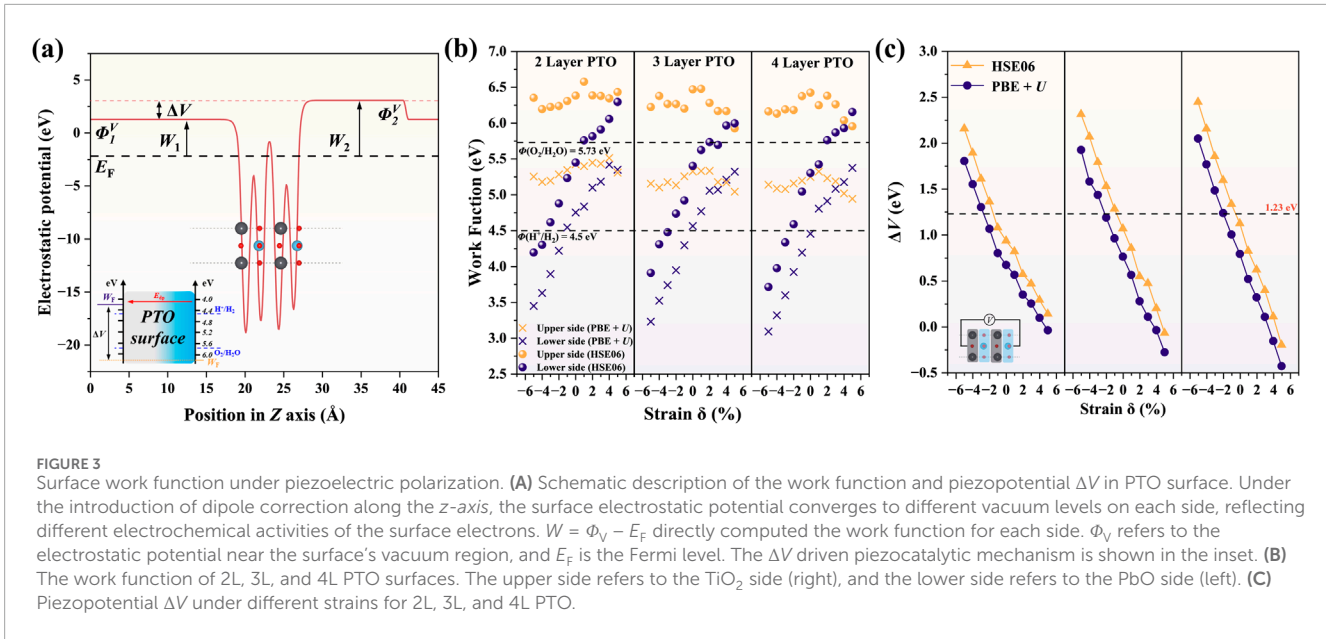
indirectly validates that thick PTO is better than thin PTO in piezocatalysis [52–54].

Finally, it is found that the correlation between  $\Delta V$  and strain  $\delta$  is nearly linear in Figure 3C. This linear relation between piezopotential and lattice strain was previously reported by Liu et al. in general piezoelectric materials, but it is derived based on a simple capacitor model with polarization along the  $z$  direction [21]. Our simulation indicates that this linear  $\Delta V$ - $\delta$  correlation also exists with the vibrational excitation in the  $xy$  plane, which enriches the mechanistic understanding of piezocatalysis.

## Piezoelectric effects on the surface adsorption of $^*H/^*OH$ group

To understand the chemical activity of piezo-electrified PTO surface, we investigate the adsorption energy of  $^*H$  and  $^*OH$  groups as examples, which are important adsorbates of the water splitting reaction. The adsorption enthalpy of an adsorbate from DFT calculation is defined by Equation 2:

$$\Delta E_A = E_{*A} - E_* - E_A, \quad (2)$$



where the index A refers to the adsorbates (H and OH groups in this work), and “\*” refers to the clean surface or active site. The total energy E can be directly obtained from DFT calculation. Considering the energy variation with the applied strain  $\delta$ , the adsorption can be written as Equation 3:

$$\begin{aligned}
 \Delta E_A(\delta) &= E_{*A}(\delta) - E_*(\delta) - E_A \\
 &= (\Delta E_{*A}(\delta) + E_{*A}(\delta = 0)) - (\Delta E_*(\delta) + E_*(\delta = 0)) - E_A \\
 &= \Delta E_{*A}(\delta) - \Delta E_*(\delta) + E_{*A}(\delta = 0) - E_*(\delta = 0) - E_A \\
 &= \Delta E_{*A}(\delta) - \Delta E_*(\delta) + \text{Constant}
 \end{aligned}
 \tag{3}$$

The  $\Delta E_A(\delta)$  refers to the strain-induced energy variation of the surface with reference to the equilibrium state. Thus, the effect of applied strain on the adsorption enthalpy can be evaluated via

the  $\Delta E^*A(\delta) - \Delta E^*(\delta)$ . We calculated the strain-induced energy variation  $\Delta E_{*A}(\delta)$  for clean, H-, and OH-absorbed PTO surfaces in Figure 4A. The clean surface exhibits larger  $\Delta E_{*A}(\delta)$  values than the H- and OH-absorbed surfaces. In addition, on the compressive strain side, the H-absorbed surface shows larger energy variation than the OH-absorbed surface, while their energy variation on the tensile strain region is very close. We further calculated the  $\Delta E^*A(\delta) - \Delta E^*(\delta)$  to evaluate the effect of strain  $\delta$  on the adsorption enthalpy, as shown in Figure 4B. One can see that either compressive or tensile strain can enhance the adsorption for both  $^*\text{H}$  and  $^*\text{OH}$  groups on PTO. This enhancement of adsorption enthalpy is nonsymmetric. Compressive strain enhances the OH adsorption more than H adsorption, while tensile strain enhances the H adsorption more than OH adsorption.

These results suggest that the chemical activity of the PTO surface can be significantly tuned via mechanical strain due to the piezoelectric effect. Here, one should note that neither excessively strong nor weak adsorption is favorable for the catalytic process. In this work, we only performed a simple analysis of the adsorption energies, but we did not conduct any detailed study on the optimal adsorption strength and its impact on the HER/OER mechanisms, which will be planned in our further work. To conclude, this strain-induced activity change should be an important part of piezocatalysis from the perspective of reaction on a molecular scale.

## Summary and conclusion

In this work, we employed the first-principles DFT calculation to study the piezocatalytic activity and mechanism of tetragonal perovskite PTO. The band structure calculation of bulk PTO shows that PTO is an indirect semiconductor with the VBM and CBM located at the X and  $\Gamma$  points in the reciprocal space. The PDOS and band decomposition of few-layer PTO indicate that the VBM and CBM were mainly contributed by the surface TiO<sub>2</sub> layer and inner TiO<sub>2</sub> layer, respectively.

Under mechanical strain, HSE06 calculation predicts an increasing  $E_g$  under compressive strain and a decreasing  $E_g$  under tensile strain, giving a monotonical trend of  $E_g$  vs.  $\delta$ . The  $E_g$  variation under strain in few-layer PTO is different from that in bulk PTO, which shows a “bell” shape across the whole region, indicating that both compressive and tensile strain leads to  $E_g$  decrease. The space charge analysis indicates that few-layer PTO is less polarized than bulk PTO due to the depolarization effect. This effect leads to a reverse electron transfer from the TiO<sub>2</sub> node to the PbO node that should effectively weaken the electronic polarization. However, an enhanced total dipole moment was observed under the compressive strain side, while the tensile strain was found to decrease the total dipole moment. This can be explained by the dominant role of the ionic dipole moment in determining the total polarization.

By looking at the surface work function and piezopotential, we found that the work function of the TiO<sub>2</sub> side (upper side) is always located beyond the H<sub>2</sub>O oxidation potential, while the work function of the PbO side is below the HER potential only when the compressive strain was introduced. The reduction potential of the PbO side can be further reduced if the thicker PTO film is used under similar strain conditions. In addition, a linear correlation exists between piezopotential  $\Delta V$  and biaxial strain  $\delta$  in the  $xy$  plane, which extends linear response ansatz to the mechanical excitation on the basal plane ( $xy$  direction) of piezoelectric perovskite.

Finally, by looking at the adsorption enthalpy change under strain, we found that both compressive and tensile strain could promote the H and OH adsorption, which should be an important part when capturing the reaction mechanism under molecular scale during piezocatalysis. Our work could provide in-depth mechanistic insight into the piezocatalytic water splitting in the piezoelectric perovskite family.

## Data availability statement

The original contributions presented in the study are included in the article/[Supplementary Material](#); further inquiries can be directed to the corresponding authors.

## Author contributions

XS: writing–original draft and writing–review and editing. XZ: conceptualization, software, validation, and writing–review and editing. EK: conceptualization, investigation, methodology, supervision, and writing–review and editing. CZ: conceptualization, funding acquisition, project administration, resources, supervision, and writing–review and editing.

## Funding

The author(s) declare that financial support was received for the research, authorship, and/or publication of this article. This work was funded by the Funding of NJUST (No. TSXK2022D002), the Natural Science Foundation of Jiangsu Province (No. BK20220929), the Natural Science Foundation of China (No. 22303039), the Fundamental Research Funds for the Central Universities (No. 30922010102), and a Startup Grant of NJUST.

## Conflict of interest

The authors declare that the research was conducted in the absence of any commercial or financial relationships that could be construed as a potential conflict of interest.

## Generative AI statement

The author(s) declare that no Generative AI was used in the creation of this manuscript.

## Publisher’s note

All claims expressed in this article are solely those of the authors and do not necessarily represent those of their affiliated organizations, or those of the publisher, the editors and the reviewers. Any product that may be evaluated in this article, or claim that may be made by its manufacturer, is not guaranteed or endorsed by the publisher.

## Supplementary material

The Supplementary Material for this article can be found online at: <https://www.frontiersin.org/articles/10.3389/fphy.2025.1562239/full#supplementary-material>

## References

- Fujishima A, Honda K. Electrochemical photolysis of water at a semiconductor electrode. *Nature* (1972) 238:37–8. doi:10.1038/238037a0
- Haryanto A, Fernando S, Murali N, Adhikari S. Current status of hydrogen production techniques by steam reforming of ethanol: a review. *Energy Fuels* (2005) 19:2098–106. doi:10.1021/ef0500538
- Seh ZW, Kibsgaard J, Dickens CF, Chorkendorff I, Nørskov JK, Jaramillo TF. Combining theory and experiment in electrocatalysis: insights into materials design. *Science* (2017) 355:eaad4998. doi:10.1126/science.aad4998
- Luo J, Zhang S, Sun M, Yang L, Luo S, Crittenden JC. A critical review on energy conversion and environmental remediation of photocatalysts with remodeling crystal lattice, surface, and interface. *ACS Nano* (2019) 13:9811–40. doi:10.1021/acsnano.9b03649
- Liu C, Chen F, Zhao B-H, Wu Y, Zhang B. Electrochemical hydrogenation and oxidation of organic species involving water. *Nat Rev Chem* (2024) 8:277–93. doi:10.1038/s41570-024-00589-z
- Wang ZL, Song J. Piezoelectric nanogenerators based on zinc oxide nanowire arrays. *Science* (2006) 312:242–6. doi:10.1126/science.1124005
- Dai B, Biesold GM, Zhang M, Zou H, Ding Y, Wang ZL, et al. Piezo-phototronic effect on photocatalysis, solar cells, photodetectors and light-emitting diodes. *Chem Soc Rev* (2021) 50:13646–91. doi:10.1039/D1CS00506E
- Deng W, Zhou Y, Libanori A, Chen G, Yang W, Chen J. Piezoelectric nanogenerators for personalized healthcare. *Chem Soc Rev* (2022) 51:3380–435. doi:10.1039/D1CS00858G
- Tu S, Guo Y, Zhang Y, Hu C, Zhang T, Ma T, et al. Piezocatalysis and piezo-photocatalysis: catalysts classification and modification strategy, reaction mechanism, and practical application. *Adv Funct Mater* (2020) 30:2005158. doi:10.1002/adfm.202005158
- Hong K-S, Xu H, Konishi H, Li X. Direct water splitting through vibrating piezoelectric microfibers in water. *J Phys Chem Lett* (2010) 1:997–1002. doi:10.1021/jz100027t
- Starr MB, Shi J, Wang X. Piezopotential-driven redox reactions at the surface of piezoelectric materials. *Angew Chem Int* (2012) Ed(51):5962–6. doi:10.1002/anie.201201424
- Wang M, Zuo Y, Wang J, Wang Y, Shen X, Qiu B, et al. Remarkably enhanced hydrogen generation of organolead halide perovskites via piezocatalysis and photocatalysis. *Adv Energy Mater* (2019) 9:1901801. doi:10.1002/aenm.201901801
- Wang Y, Wen X, Jia Y, Huang M, Wang F, Zhang X, et al. Piezo-catalysis for nondestructive tooth whitening. *Nat Commun* (2020) 11:1328. doi:10.1038/s41467-020-15015-3
- Su R, Hsain HA, Wu M, Zhang D, Hu X, Wang Z, et al. Nano-ferroelectric for high efficiency overall water splitting under ultrasonic vibration. *Angew Chem Int* (2019) Ed(58):15076–81. doi:10.1002/anie.201907695
- Zhang A, Liu Z, Xie B, Lu J, Guo K, Ke S, et al. Vibration catalysis of eco-friendly  $\text{Na}_{0.5}\text{K}_{0.5}\text{NbO}_3$ -based piezoelectric: an efficient phase boundary catalyst. *Appl Catal B* (2020) 279:119353. doi:10.1016/j.apcatb.2020.119353
- Wang Y-C, Wu JM. Effect of controlled oxygen vacancy on  $\text{H}_2$ -production through the piezocatalysis and piezophotonics of ferroelectric  $\text{R}_3\text{C ZnSnO}_3$  nanowires. *Adv Funct Mater* (2020) 30:1907619. doi:10.1002/adfm.201907619
- Kubota K, Pang Y, Miura A, Ito H. Redox reactions of small organic molecules using ball milling and piezoelectric materials. *Science* (2019) 366:1500–4. doi:10.1126/science.aay8224
- Wu M-H, Lee J-T, Chung YJ, Srinivas M, Wu J-M. Ultrahigh efficient degradation activity of single- and few-layered  $\text{MoSe}_2$  nanoflowers in dark by piezo-catalyst effect. *Nano Energy* (2017) 40:369–75. doi:10.1016/j.nanoen.2017.08.042
- Wang K, Han C, Li J, Qiu J, Sunarso J, Liu S. The mechanism of piezocatalysis: energy band theory or screening charge effect? *Angew Chem Int* (2022). doi:10.1002/anie.202110429
- Starr MB, Wang X. Fundamental analysis of piezocatalysis process on the surfaces of strained piezoelectric materials. *Sci Rep* (2013) 3:2160. doi:10.1038/srep02160
- Liu Z, Wang B, Chu D, Cazorla C. First-principles high-throughput screening of bulk piezo-photocatalytic materials for sunlight-driven hydrogen production. *J Mater Chem A* (2022) 10:18132–46. doi:10.1039/D2TA05941J
- Zhou Z, Zhan C, Kan E. Understanding the piezocatalytic properties of the  $\text{BaTiO}_3(001)$  surface via density functional theory. *Phys Chem Chem Phys* (2023) 25:8631–40. doi:10.1039/D2CP05631C
- Su R, Wang Z, Zhu L, Pan Y, Zhang D, Wen H, et al. Strain-engineered nano-ferroelectrics for high-efficiency piezocatalytic overall water splitting. *Angew Chem Int* (2021) Ed(60):16019–26. doi:10.1002/anie.202103112
- Zhu P, Chen Y, Shi J. Piezocatalytic tumor therapy by ultrasound-triggered and  $\text{BaTiO}_3$ -mediated piezoelectricity. *Adv Mater* (2020) 32:2001976. doi:10.1002/adma.202001976
- Starr MB, Wang X. Coupling of piezoelectric effect with electrochemical processes. *Nano Energy* (2015) 14:296–311. doi:10.1016/j.nanoen.2015.01.035
- Kresse G, Furthmüller J. Efficiency of ab-initio total energy calculations for metals and semiconductors using a plane-wave basis set. *Comput Mater Sci* (1996) 6:15–50. doi:10.1016/0927-0256(96)00008-0
- Kresse G, Furthmüller J. Efficient iterative schemes for ab initio total-energy calculations using a plane-wave basis set. *Phys Rev B* (1996) 54:11169–86. doi:10.1103/PhysRevB.54.11169
- Blöchl PE. Projector augmented-wave method. *Phys Rev B* (1994) 50:17953–79. doi:10.1103/PhysRevB.50.17953
- Hammer B, Hansen LB, Nørskov JK. Improved adsorption energetics within density-functional theory using revised Perdew-Burke-Ernzerhof functionals. *Phys Rev B* (1999) 59:7413–21. doi:10.1103/PhysRevB.59.7413
- Perdew JP, Burke K, Ernzerhof M. Generalized gradient approximation made simple. *Phys Rev Lett* (1996) 77:3865–8. doi:10.1103/PhysRevLett.77.3865
- Grimme S, Antony J, Ehrlich S, Krieg H. A consistent and accurate ab initio parametrization of density functional dispersion correction (DFT-D) for the 94 elements H-Pu. *J Chem Phys* (2010) 132:154104. doi:10.1063/1.3382344
- Chadi DJ, Cohen ML. Special points in the Brillouin zone. *Phys Rev B* (1973) 8:5747–53. doi:10.1103/PhysRevB.8.5747
- Majumder S, Basera P, Tripathi M, Choudhary RJ, Bhattacharya S, Bapna K, et al. Elucidating the origin of magnetic ordering in ferroelectric  $\text{BaTiO}_{3-\text{D}}$  thin film via electronic structure modification. *J Phys Condens Matter* (2019) 31:205001. doi:10.1088/1361-648X/ab06d5
- Heyd J, Scuseria GE, Ernzerhof M. Hybrid functionals based on a screened coulomb potential. *J Chem Phys* (2003) 118:8207–15. doi:10.1063/1.1564060
- Becke AD. Density-functional thermochemistry. Iii. The role of exact exchange. *J Chem Phys* (1993) 98:5648–52. doi:10.1063/1.464913
- Sági-Szabó G, Cohen RE, Krakauer H. First-principles study of piezoelectricity in  $\text{PbTiO}_3$ . *Phys Rev Lett* (1998) 80:4321–4. doi:10.1103/PhysRevLett.80.4321
- Bendaoudi L, Ouahrani T, Daouli A, Rerbal B, Boufatah RM, Morales-García Á, et al. Electronic and electrocatalytic properties of  $\text{PbTiO}_3$ : unveiling the effect of strain and oxygen vacancy. *Dalton Trans* (2023) 52:11965–80. doi:10.1039/D3DT01478A
- Neugebauer J, Scheffler M. Adsorbate-substrate and adsorbate-adsorbate interactions of Na and K adlayers on  $\text{Al}(111)$ . *Phys Rev B* (1992) 46:16067–80. doi:10.1103/PhysRevB.46.16067
- King-Smith RD, Vanderbilt D. Theory of polarization of crystalline solids. *Phys Rev B* (1993) 47:1651–4. doi:10.1103/PhysRevB.47.1651
- Perdew JP, Ruzsinszky A, Csonka GI, Vydrov OA, Scuseria GE, Constantin LA, et al. Restoring the density-gradient expansion for exchange in solids and surfaces. *Phys Rev Lett* (2008) 100:136406. doi:10.1103/PhysRevLett.100.136406
- Gebreyesus G, Bastonero L, Kotiuga M, Marzari N, Timrov I. Understanding the role of hubbard corrections in the rhombohedral phase of  $\text{BaTiO}_3$ . *Phys Rev B* (2023) 108:235171. doi:10.1103/PhysRevB.108.235171
- Mabud SA, Glazer AM. Lattice parameters and birefringence in  $\text{PbTiO}_3$  single crystals. *J Appl Crystallogr* (1979) 12:49–53. doi:10.1107/S0021889879011754
- Wójcik K. Electrical properties of  $\text{PbTiO}_3$  single crystals doped with lanthanum. *Ferroelectrics* (1989) 99:5–12. doi:10.1080/00150198908221435
- Li Z, Grimsditch M, Xu X, Chan SK. The elastic, piezoelectric and dielectric constants of tetragonal  $\text{PbTiO}_3$  single crystals. *Ferroelectrics* (1993) 141:313–25. doi:10.1080/00150199308223459
- Lemziouka H, Omari LEH, Moubah R, Boutahar A, Bahhar S, Abid M, et al. Structural, dielectric and optical properties of Cu-doped  $\text{PbTiO}_3$  ceramics prepared by sol-gel. *Mater Today Proc* (2021) 37:3940–5. doi:10.1016/j.matpr.2020.09.094
- Prajapati P, Singh AK. Band gap tuning of ferroelectric  $\text{PbTiO}_3$  by Mo doping. *J Mater Sci: Mater Electron* (2022) 33:2550–65. doi:10.1007/s10854-021-07461-6
- Berger RF, Fennie CJ, Neaton JB. Band gap and edge engineering via ferroic distortion and anisotropic strain: the case of  $\text{SrTiO}_3$ . *Phys Rev Lett* (2011) 107:146804. doi:10.1103/PhysRevLett.107.146804
- Tang W, Sanville E, Henkelman G. A grid-based bader analysis algorithm without lattice bias. *J Phys Condens Matter* (2009) 21:084204. Epub 20090130. doi:10.1088/0953-8984/21/8/084204

49. Vonrüti N, Aschauer U. Epitaxial strain dependence of band gaps in perovskite oxynitrides compared to perovskite oxides. *Phys Rev Mater* (2018) 2:105401. doi:10.1103/PhysRevMaterials.2.105401
50. Parker WD, Rondinelli JM, Nakhmanson SM. First-principles study of misfit strain-stabilized ferroelectric  $\text{SnTiO}_3$ . *Phys Rev B* (2011) 84:245126. doi:10.1103/PhysRevB.84.245126
51. Jung S, Pizzolitto C, Biasi P, Dauenhauer PJ, Birol T. Programmable catalysis by support polarization: elucidating and breaking scaling relations. *Nat Commun* (2023) 14:7795. doi:10.1038/s41467-023-43641-0
52. Amiri O, Salar K, Othman P, Rasul T, Faiq D, Saadat M. Purification of wastewater by the piezo-catalyst effect of  $\text{PbTiO}_3$  nanostructures under ultrasonic vibration. *J Hazard Mater* (2020) 394:122514. doi:10.1016/j.jhazmat.2020.122514
53. Wan G, Yin L, Chen X, Xu X, Huang J, Zhen C, et al. Photocatalytic overall water splitting over  $\text{PbTiO}_3$  modulated by oxygen vacancy and ferroelectric polarization. *J Am Chem Soc* (2022) 144:20342–50. doi:10.1021/jacs.2c08177
54. Huang X, Lei R, Yuan J, Gao F, Jiang C, Feng W, et al. Insight into the piezo-photo coupling effect of  $\text{PbTiO}_3/\text{CdS}$  composites for piezo-photocatalytic hydrogen production. *Appl Catal B* (2021) 282:119586. doi:10.1016/j.apcatb.2020.119586